Floating Bare Tether as Upper Atmosphere Probe

J. R. Sanmartín, M. Charro, J. Peláez and I. Tinao
Universidad Politécnica de Madrid, Madrid 28040, *Spain*

S. Elaskar,
Conicet, Universidad Nacional de Córdoba, Córdoba, Argentina

A. Hilgers,
ESTEC - European Space Agency, Noordwijk, Netherlands

Use of a (bare) conductive tape electrically floating in LEO as an effective e-beam source that produces artificial auroras, and is free of problems that have marred standard beams, is considered. Ambient ions impacting the tape with KeV energies over most of its length liberate secondary electrons, which race down the magnetic field and excite neutrals in the E-layer, resulting in auroral emissions. The tether would operate at night-time with both a power supply and a plasma contactor off; power and contactor would be on at daytime for reboost. The optimal tape thickness yielding a minimum mass for an autonomous system is determined; the alternative use of an electric thruster for day reboost, depending on mission duration, is discussed. Measurements of emission brightness from the spacecraft could allow determination of the (neutral) density vertical profile in the critical E-layer; the flux and energy in the beam, varying along the tether, allow imaging line-of-sight integrated emissions that mix effects with altitude-dependent neutral density and lead to a brightness peak in the beam footprint at the E-layer. Difficulties in tomographic inversion, to determine the density profile, result from beam broadening, due to elastic collisions, which flattens the peak, and to the highly nonlinear functional dependency of line-of-sight brightness. Some dynamical issues are discussed.

I. Introduction

A conductive tether left uninsulated and electrically floating in LEO could serve as effective electron beam source to produce artificial auroras. Standard e-beams emitted from satellites are marred by satellite-charging problems and have small cross-sections (radius about one electron-gyroradius at KeV energies), requiring ground observation made possible by a beam energy-flux two orders of magnitude greater than in the strongest natural auroras; this compensates for the thinness of the emitting layer but results in gross beam distortions by nonlinear plasma effects. In addition, the gross perturbations produced by the intense beam emission in the space plasma around the spacecraft affect emission itself, and the luminous glow arising from electron bombardment in the return current contaminates sensitive optical instruments.

Because of the large ion-to-electron mass ratio, an electrically floating tether is biased highly negative over most of its length by the motional electric field. Ions impacting with keV energies liberate secondary electrons that accelerate away through the 2D local bias, race down magnetic lines, and result in peak auroral emissions in the E-layer. Since no current flows at tether ends the e-beam is free of spacecraft charging problems. The beam is also free of plasma-interaction problems: its very large cross section (twice electron-gyroradius $\times$ tether length) results in energy flux over 10^3 times weaker than in standard beams. In addition, emission of such a weak flux has no significant effect on the local plasma, and takes place far from any instrument. Beyond auroral effects proper, observations along the beam, from a spacecraft carrying a floating bare-tether, might provide real-time mapping of E-layer neutral density, of interest in numerical simulations of the atmosphere lying below, and in orbit decay and reentry predictions.[1]

II. Tether System Design

The tether operates at night-time, with power supply and a Hollow Cathode (HC) off, for current to vanish at both tether ends. For an eastward moving S/C, electrons are collected above a zero-bias point very near the top; each ion collected below picks up an electron to leave as neutral, electrons thus leaking out at the (OML) ion-impact rate increased by secondary emission with yield proportional to bias. Because ion collection is slow, ohmic effects are weak, a floating tether being near equipotential (**Fig.1**).

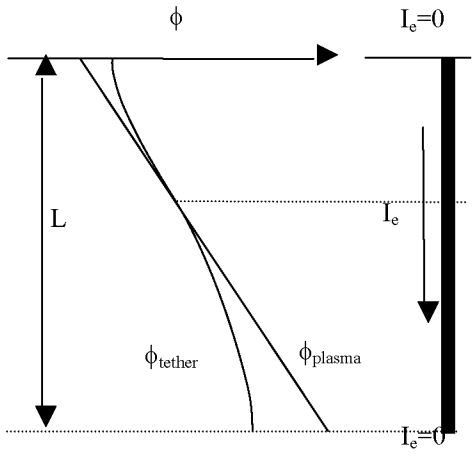

Fig.1 Profiles of plasma and tether potentials at night.

With full bias proportional to tether length L, the OML ion current varies as $wL \times \sqrt{L}$ for a thin tape of width w; the total emitted secondary current, gauging beam performance, varies as $wL^{3/2} \times L$. Width w should be large to reduce the probability of cuts by debris, which increases with mission duration, but small enough to allow the tape to collect current in the OML regime (w less than about 25 mm). Beam flux and footprint at the E-layer vary as wL and $L \times \sqrt{L}$ respectively (electron gyroradius, being proportional to square root of energy, varies as $\sqrt{L}$ at the start of the race down the magnetic field). Greater energy ($\sim L$) allowing deeper penetration down the E-layer, column-integrated (line-of-sight) emission rates roughly vary as $wL \times L$.

The electron current at night flows downwards throughout the tether, resulting in magnetic drag. Power and HC at the top would be on at daytime, to partially reverse the current and reboost the spacecraft once per orbit, making the tether an autonomous e-beam source. Above some zero-current point, electron current flows and increases upwards to leave at the HC, and produces thrust; conditions below that point are as at night, resulting in drag. The supply power must produce thrust enough to balance the night and day drag.[2] (**Fig. 2**)

Drivers for tether material properties are density low and conductivity high, leading to use of aluminum. Whatever w and L, the mass of a tape can be reduced by making it thinner. There exists, however, an optimal thickness δ yielding minimum system mass, which, for limited mission times, is made of mass related to the power subsystem and remaining hardware mass. At large enough δ, tether-related hardware mass, which accounts for end-mass/deployer and tether itself, and is just taken proportional to tether mass $\sim Lw\delta$, would be clearly dominant. At small enough δ, mass of power-subsystem (HC/Power Processing Unit/Solar Array, counting as low as 20 kg/kw) would be dominant: a tape very thin and thus having a large ohmic resistance, requires a large solar array to push current through. Thrust power would be proportional to *motional field* $\times$ *current* $\times L$, scaling as $wL^{5/2}$ in case ohmic effects did not reduce current below OML values ($\sim wL^{3/2}$). One would then have

$$\frac{power-subsystem\ mass}{tether-hardware\ mass} \sim \frac{wL^{5/2}}{Lw\delta} \sim \frac{L^{3/2}}{\delta} \qquad \text{(if no ohmic effects)} \qquad (1)$$

Ohmic effects on thrust are strong, however (effects on day drag are sensible too). Ohmic effects are gauged by the ratio between OML current and short circuit current (*conductivity* $\times$ *motional field* $\times$ *cross-secion area*), which also scales as $L^{3/2}/\delta$,

$$\frac{OML\ current}{Short-circuit\ current} \sim \frac{wL^{3/2}}{w\delta} \sim \frac{L^{3/2}}{\delta}. \qquad (2)$$

For typical orbit day/night conditions, the minimum in overall mass occurs at a definite value of the ratio $L^{3/2}/\delta$ in (1) and (2),

$$\delta = 0.18 \text{ mm} \times (\text{L} / 20 \text{ km})^{3/2} \quad \rightarrow \quad \text{minimum mass} \sim \text{wL}^{3/2}. \tag{3}$$

The *power-subsystem/hardware* mass ratio is then about 1.7 and the *efficiency* ≡ *magnetic-thrust power/solar array power* about 0.17.

A tape of width 12 mm would have a mass 116.6 kg; for hardware mass 3 times as large, total system mass would be 945 kg. The electric power required would be 29.8 kw, supply voltage and current being 1.09kV and 27.3 A respectively. Since minimum system mass, scaling as $wL^{5/2}$, increases fast with tether length, the range of design values for L is narrow (15-25km) because column-integrated ionization rates ($\sim wL^2$) decrease rapidly with tether length.

HC-expellant mass might in principle need be considered in the case of long enough missions. Consumption rate is very low, however. Mass-flow rate and electron current in a state-of-the-art HC allow ascribing a "specific impulse" to ED-tethers in LEO that is over 10^2 times greater than the specific impulse of an Ion Thruster.[3] For our optimal auroral-probe tether, expellant mass would take 180 months to be as large as power subsystem mass.

The solar array could be used to feed power to an Ion thruster, which would then provide thrust.[4] With typical (propulsive) *efficiency* $\eta_{IT} \sim 0.65$ and exhaust velocity $v_{exh} \sim 30$ km/s, the effective *efficiency* of the Ion Thruster would here be, $\eta_{IT} \times 2v_{orb}/v_{exh} \approx 0.32$, reducing system mass through savings in the power-subsystem mass due to the efficiency gain factor $0.32/0.17 \approx 1.88$; on the other hand, the full tether would now exert day-drag, and the Ion Thruster would be heavier than a HC. A thinner tape could reduce hardware mass with no effect on the power subsystem, but incipient ohmic effects at night would reduce auroral effects. Further, Ion Thrusters consume mass at a much faster rate than a HC and become comparatively less convenient the longer the mission. For a mission reaching beyond a few months, use of the tape-tether itself for day-thrust will always result in a system lighter than a system using an Ion Thruster.

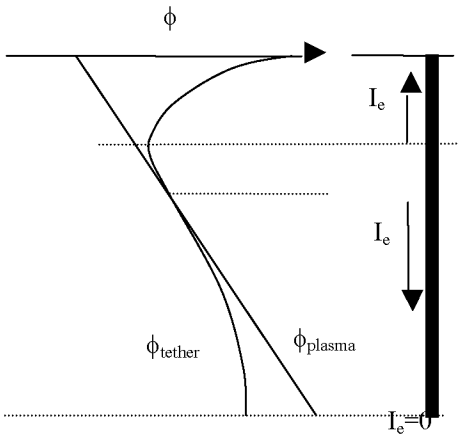

Fig.2 Profiles of plasma and tether potentials at daytime. Power supply at the top gets the electron current across to the Hollow Cathode.

During the night in orbit, the electrodynamic torque is extremely small (it can be made to vanish by a proper distribution of top and bottom masses) and the tether keeps very straight and vertical. Although the day torque cannot be made to vanish, it is small; the skip rope instability would take 10 years to develop.[5] Deploying our metallic tape without a flexible leader would require keeping friction inside the deployer under well defined limits.

III. Beam-atmosphere Interaction

Each point in the tether emits monoenergetic secondary electrons, both electron energy ε_0 and flux Φ_0 increasing linearly with distance h from the top. Beam half-width perpendicular to the tether varies as $\sqrt{h}$. With the electric potential shallow for some distance from the tether, e-beam electrons are near uniformly distributed in azimuth when reaching the undisturbed plasma; this results in a definite pitch-angle θ distribution involving the (dip) angle I between magnetic line and horizontal plane $F_0(\theta)$, (**Fig. 3**).

As beam electrons move in helical paths down magnetic lines, they find a density of neutral molecules $n(z)$ increasing with decreasing altitude. Beam electrons lose energy in inelastic ionization and excitation collisions, followed by photon emission. Electron energy at any altitude depends on the density profile above, the h value at emission, and the pitch angle,

$$\varepsilon = \varepsilon (z; h, \theta); \tag{4}$$

electrons at low pitch penetrate further down. Beam electrons are also scattered in elastic collisions with air molecules, which both affect pitch distribution and reduce beam flux by some width-broadening factor f_{br} due to diffusion across magnetic lines,

$$\Phi \approx \Phi_0(\text{h}) / \text{f}_{\text{br}} [\varepsilon ; \varepsilon_o(\text{h})] \tag{5}$$

Simple, opposite models for the evolution in the pitch distribution, $F(\theta)$ [distribution frozen in initial form and uniform distribution reached immediately after leaving the tether and kept afterwards], show somewhat similar results.

The pitch-averaged, volumetric ionization rate is proportional to beam flux, local density, and ionization cross-section, which is just energy dependent,

$$\dot{n}_i(z,\, h) \;=\; \int d\theta\, F(\theta) \frac{\Phi_0(h)}{f_{br}\left[\varepsilon(z;h,\theta);\; \varepsilon_0(h)\right]} n(z)\, \sigma_i\left[\varepsilon(z;h,\theta)\right]. \qquad (6)$$

With beam thick 250m at most, dwell-time at any particular point is much less than buildup time for the electron population density to reach a steady state. However, excited states with prompt emission through *allowed* transitions do reach a steady-state, emission rates then being proportional to excitation rates. Since cross sections have similar energy dependence for all collisional interactions, there exist simple approximate relations between emission and ionization rates for prominent spectral bands and lines, under some standard conditions.

IV. Observational Scheme

Observations from the spacecraft (at about 300 km altitude, to be close to the F-layer maximum while keeping away from the ISS) involve 'column'-integrated emission rates along straight lines extending over the ionization region and determining a relation $h\,(z,\, \psi)$,

$$b_\psi \;=\; \int \dot{n}_i\, ds\,, \qquad\qquad ds \;=\; -dz \,/\, sin\,(I+\psi) \qquad (7)$$

Surface brightness b as measured in Rayleigh units, at each small angle ψ from the magnetic field, mix altitude-z /h-value effects. As a result, the narrow emission footprint of the beam, which is tens of kilometers long and covers a line-of-sight range of about 6°, shows a peak in brightness that is about $10^2\, R$ for prominent bands and lines. Footprint length is greater for a 45° dip, varying little over a large part of a middle-inclination orbit.

Observations will use CCD cameras, a refractive system being lighter, simpler and allowing a wider field of view than a reflective one. For easier alignment, the angular field-of-view could be twice the angle subtended by the emission footprint, or about 12°. It clearly proves convenient to have a large number of pixels of large size on each side of the CCD detector; 10^3 30 μm-pixels make for a detector side of 30 mm, a 12° field-of-view then requiring a focal length of 15 cm. One could easily tile 9 10 mm x 10 mm chips to get a detector of 30 mm x 30 mm.

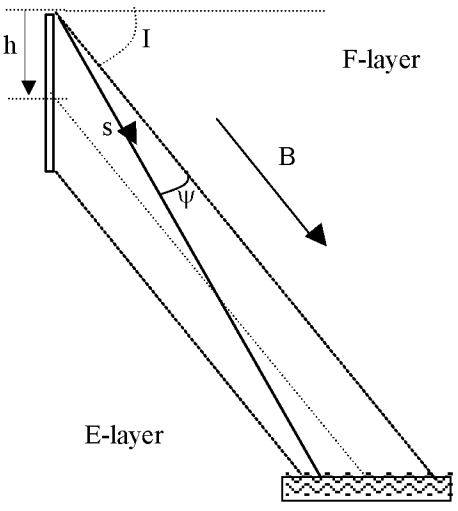

Fig.3 Geometrical disposition of tether and magnetic field.

Brightness of 30-100 R is well above background noise, and noise from present values of dark current prove completely negligible; critical noise arises from the CCD readout. To get a large signal-to-noise ratio, the number of photons incident on a pixel must be large, requiring large pixels but also an entrance aperture subtending a large solid angle at the detector, and a long exposure time, which is limited by satellite motion. For a 0.1 s exposure (atmospheric emission being reasonable homogeneous over 750 m satellite displacements), a f-ratio as low as 1, a 30 μm pixel, and 0.5 optics transmission, brightness of 30-100 R yields 1-3 photons per pixel, say, a charge packet of two electrons for present quantum efficiencies close to 100%. Though the image is narrow across the footprint, it still covers about 5 pixels, allowing use of a binning mode that sums photons gathered by nearby pixels across the image with no increase in readout noise, to yield a 10-electron packet. The S/N ratio is too low, however, even with recent techniques yielding sub-electron readout. A S/N ratio

~ 10^2 will require use of *Image Intensifiers*, which are complex and costly but achieve net signal gains of about 1000.

The signal for ground observation across the beam could provide direct vertical resolution of the density profile but is too weak (*brightness* ~ 1 *R*). Pulsing a HC located at tether bottom to allow electrons to escape there after collection over the length of the tether could increase the *S/N* ratio, but requires, however, to locate a second HC and subsystems at the bottom, away from the power source; also, night drag would greatly increase during HC-on periods. Independently, transients in the bias/current pulse travelling along the tether could affect its workings as an e-beam source. Modelling the tether as a transmission line, with a (no-loss) phase velocity close to the light velocity, the time for a pulse to travel down the line (6×10^{-5} s, for L = 20 km) is comparable to the time response of ambient oxygen ions to changes in bias (a few times 10^{-5} s, for a 10^5 cm^{-3} electron density). Again, with tether resistance (~ 250 Ω) comparable to the (no-loss) line impedance, a pulse should be strongly attenuated as it travels down the line.

V. Tomographic Inversion

In a first simple scheme, the camera would operate on the 391.4 nm (or the 427.8 nm) spectral band to determine the N_2-density, and the 777.4 nm and 844.6 nm lines, with definite branching ratios, to determine O_2-

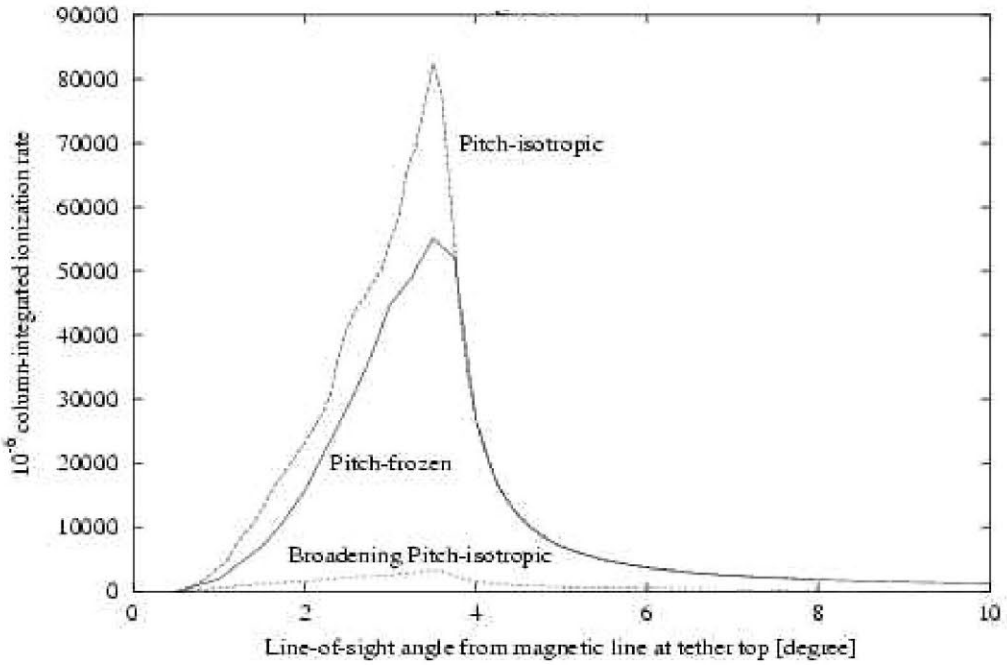

Fig.4 **Column-integrated ionization rates for frozen and isotropic pitch distributions with no beam broadening and isotropic pitch with broadening.**

and *O*-densities, using three interference filters controlled by hardware to switch rapidly from one wavelength to another. An alternative would be using three cameras, each with a single filter. A third possibility would use a grating for a spectral separation of the incoming radiation. The narrow footprint would allow non-overlapping images at different wavelengths, a dimension of the array providing spectral information and the other dimension spatial information.

The tomography problem is complex. Line-of-sight measurements are here taken from one location instead of combining information from several (ground) stations. Standard convolution algorithms do no apply to a nadir-scan, which is here the case; backscatter effects may be fully ignored, however. The unknowns would be density values at a number of altitudes equal to the number of pixels along one side of the CCD detector, each pixel corresponding to a line-of-sight. An iterative solution scheme uses density values at step m in evaluating a $10^3 \times 10^3$ linearized kernel matrix to determine densities at step $m + 1$. The kernel is found to be numerically singular, however, for any reasonable density profile; this is a result of broadening having flattened considerably the peak in brightness versus

line-of-sight (**Fig. 4**). A (Singular-Value-Decomposition) regularization technique does allow to proceed with the inversion.[6]

Iteration, however, does not converge if the initial guess for the density profile differs substantially from the actual profile; this appears to be a result from the highly nonlinear dependence of the kernel on density. Tomographic inversion is then carried in two steps. A direct approximation to the actual density profile is obtained by fitting parameters in a model and using a Direction Set (Powell) technique.[7] This estimate is then used as initial guess in the kernel, to start the iteration of the regularized inversion process.

Acknowledgments

This work was carried out under a Contract with the European Space Agency at ESTEC, Noordwijk, Netherlands. J. R. Sanmartin would like to thank Dr. M. Martínez-Sánchez for useful discussions on multiple issues concerning the proposed bare-tether probe.

References

[1]Martinez-Sanchez, M. and Sanmartin, J.R., "Artificial auroral effects from a bare conducting tether", *Journal of Geophysical Research*, Vol. 102, No. A12, 1997, pp. 27257-27263; Sanmartin, J.R., Ahedo, E., and Martinez-Sanchez, M., "An Upper Atmospheric Probe for Auroral Effects", *Proceedings 7th Spacecraft Charging Technology Conference*, ESA, Noordwijk, 2001, pp. 315-320.

[2]Sanmartin, J.R., Charro, M., Elaskar, S., Pelaez, J., Tinao, I., and Hilgers, A., "Floating Bare Tether as Upper Atmosphere Probe", Final Report, ESA, Noordwijk, February 2004.

[3]Sanmartin, J.R., Estes, R.D., and Lorenzini, E.C., "Efficiency of Different types of ED-Tether Thrusters", *Space Technology and Applications International Forum 2001*, edited by M. S. El-Genk, American Institute of Physics, New York, 2002, pp. 479-487; Estes, R.D., Lorenzini, E.C., and Sanmartin, J.R., "Short Tethers for Electrodynamic Thrust", *Space Technology and Applications International Forum 2002*, edited by M. S. El-Genk, American Institute of Physics, New York, 2002, pp. 526-533.

[4]Martinez-Sanchez, M., and Pollard, J.E., "Spacecraft Electric Propulsion - An Overview", *Journal of Propulsion and Rockets*, Vol. 14, No. 5, 1988, pp. 688-699.

[5]Pelaez, J., Lorenzini, E.C., Lopez-Rebollal, O., and Ruiz, M., "A New Kind of Dynamic Instability in Electrodynamic Tethers", *The Journal of Astronautical Sciences*, Vol. 48, No. 4, 2000, pp. 449-476.

[6]Herman, G.T., Tuy, H.K., Langenberg, K.J., and Sabatier, P.C., *Basic Methods of Tomography and Inverse Problems*, ed. by P.C. Sabatier, Adam Hilger, Bristol and Philadelphia, 1987.

[7]Press, W.H., Teukolsky, S.A., Vetterling, W.T., and Flannery, B.P., *Numerical Recipes in C*, 2nd ed., Cambridge University, Cambridge, 1988.